Contents

1. Cyclotron 1

1.1 Introduction 1
1.2 Classical cyclotron 7
1.2.1 Fixed-energy orbits, revolution period 7
1.2.2 Weak focusing 9
1.2.3 Coordinate transport 13
1.2.4 Resonant acceleration 15
1.3 Relativistic cyclotron 17
1.3.1 Thomas focusing 18
1.3.2 Spiral sector 23
1.3.3 Isochronous acceleration 24
1.4 summary 24
1.5 Appendix 26
1.5.1 Field map and optical sequence for Exercise 1.1-1 26
1.5.2 Optical sequence for Exercise 1.2.1-1.c 27

Chapter 1

Cyclotron

In addition to the cyclotron accelerator, this first chapter introduces preliminary beam optics notions, including orbit, field index, periodic stability, optical functions, together with a key optical element: the dipole magnet. These concepts will be manipulated throughout the course. The chapter also familiarizes with ray-tracing and computer program simulations, starting with short, simple, optical sequences.

1.1 Introduction

The cyclotron arrived at a time, ∼1930 [1] (Fig. 1.1), where techniques to accelerate ions were sought, for the study of nuclear properties of the atom. To this day, hundreds of cyclotrons have been built, and more still are, to accelerate protons, ions, radioactive isotopes. They find application in "particle factories" (production of high flux beams of muons, neutrons, etc., Fig. 1.2), protontherapy (Fig. 1.3), production of radio-isotopes for medicine, and more. Cryogeny technologies allow further progress towards compactness (Fig. 1.3), and towards higher rigidities [2] (Fig. 1.4).

The cyclotron combined together two long known concepts: resonant acceleration through electric gaps, and trajectory bending by a magnetic field. It was conceived as a means to overcome the inconvenient of using a long series of high voltage electrodes in a linear layout, by, instead, repeated recirculation using a magnetic field, for incremental, resonant, energy gain through a single accelerating gap. This gap is formed by a pair of cylindrical electrodes, the "dees" (Figs. 1.5). which are applied a fixed frequency oscillating voltage, generated using a radio transmitter. The dees are plunged in a uniform magnetic field which causes the ion bunches to follow, as they are accelerated, a piecewise-circular path with increasing

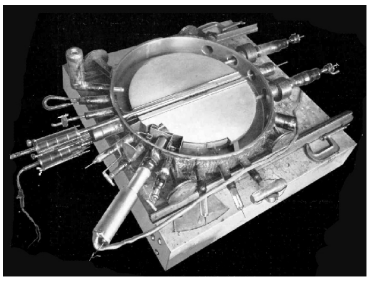

Fig. 1.1 An early cyclotron, late 1930s.

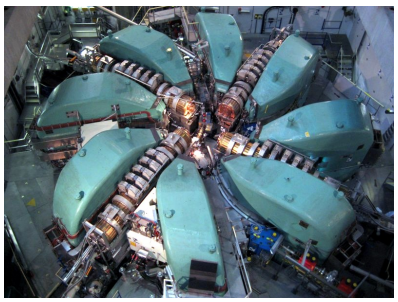

Fig. 1.2 The high power CW proton cyclotron at PSI, 1.4 MW today steadily increasing with years. It delivers a 590 MeV beam for secondary particle production (*e.g.*, neutron, muon).

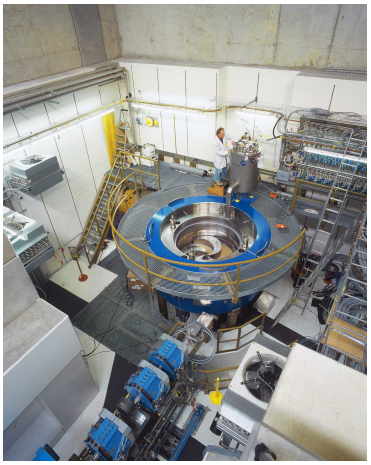

Fig. 1.3 Superconducting-coil isochronous spiral-sector AVF cyclotron at PSI, providing 250 MeV, 500 nA beams for hadrontherapy.

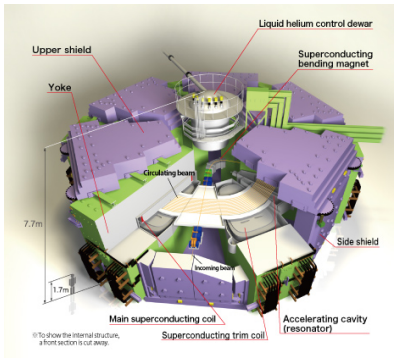

Fig. 1.4 RIKEN superconducting-coils separated-sector K*** heavy ion cyclotron, a compact, $\sim$ 20 m diameter, K-***, *** GeV proton equivalent rigidity [**?**] [**?**].

radius, normal to the field, in synchronism with the voltage oscillation. Here lies the cyclotron idea: while an accelerated bunch spirals outward, the increase in the distance it travels over a turn is compensated by its velocity increase: in the non-relativistic approximation ($\gamma \approx 1$), the revolution time T_{rev} remains quasi-constant; with the appropriate voltage frequency

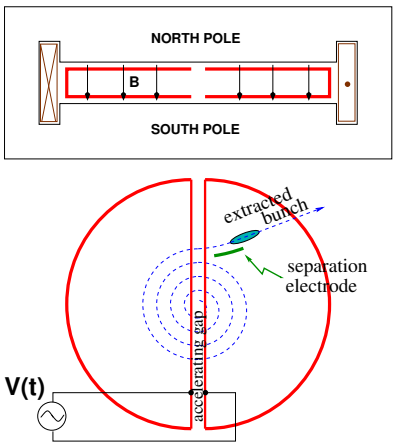

Fig. 1.5 Cyclotron : trajectories spiral in the uniform magnetic field between two circular poles. A double-dee forms a gap which is applied an oscillating voltage V(t) with frequency an integer multiple h of the revolution frequency, causing particles with the proper phase with respect to V(t) to be accelerated at each crossing. Bunch extraction is obtained by way of a separation electrode, located in the region etween the last two turns. *In passing: check the consistency of the coil current, direction of* $\vec{B}$ *and particle rotation - what is the sign of the accelerated particles?*

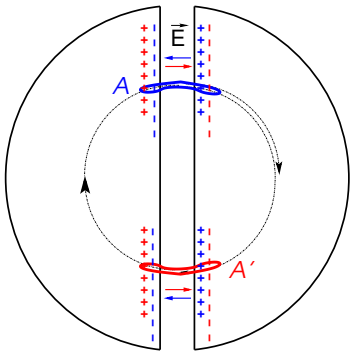

Fig. 1.6 Resonant acceleration: a bunch meeting an accelerating field $\vec{E}$ across the gap at A, at time t, will meet again, half a revolution later, at time $t + T_{rev}/2 = t + hT_{RF}/2$, an accelerating field $\vec{E}$ across the gap at A', and so forth turn after turn.

$f_{RF} \approx h/T_{rev}$ revolution motion and RF can be maintained in close synchronism, Trev $\approx hT_{RF}$, so that the bunch transit the accelerating gaps during the accelerating phase of V(t) (Fig. 1.6).

• **Exercise 1.1-1.** *Modeling a magnet using a field map, ray-tracing in that magnet, checking geometrical and dynamical outcomes against theory.*

Note 1: The optical sequence in zgoubi, for this exercise, is given in appendix 1.5.1 It uses (see *Zgoubi Users's Guide*), (i) `OBJET` to define a reference rigidity and to define the initial particle coordinates; (ii) `TOSCA` to read the field map and track through step-by-step (and `TOSCA`'s '`IL=2`' flag to store step-by-step particle data into zgoubi.plt); (iii) `FAISCEAU` to print out particle coordinates in zgoubi.res, or `FAISTORE` to print out in *e.g.* zgoubi.fai.

Note 2: A short fortran program that generates the 180 degree field map needed, is given in App. 1.5.1.

1.a - Construct a 180-degree 2-dimensional map of the field $B(R, \theta)$ in the

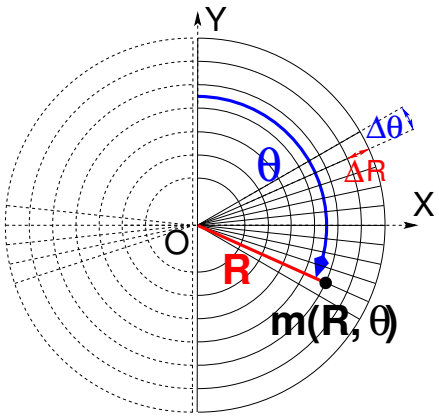

Fig. 1.7 A sketch of a cylindrical field map mesh, *i.e.*, a set of $m(R, \theta)$ nodes in a frame (O, X, Y), covering 180^0 (solid lines). The median plane field map so defined, namely the set of vertical field component values $B_Z(R, \theta)$ at the nodes of the mesh, represents a half of the cyclotron dipole; using it twice (additional 180^0 dashed line mesh) allows covering the all 360^o dipole. The mesh nodes are distant ΔR radially, $\Delta\theta$ in angle. Note: fabricating a 2D median plane field map is an easy way to define a magnetic field distribution for ray-tracing, often useful when an accurate analytical modeling is not available at hand.

plane located half-way between the north and south poles in Fig. 1.5. (the "median plane"). Use a uniform mesh in a cylindrical coordinate system (R, θ), covering R=1 to 76 cm. Zgoubi requires a reference radius as part of the field map data, a convenient value is $R_M = 50$ cm. The radial increment of the mesh is $\Delta R = 0.5$ cm, the axial increment is $\Delta\theta = 0.5\,\mathrm{cm/RM}$. Take constant axial field B = 0.5 T. The storage file, to be read by the tracking code, will have the following formatting, 6 columns:

$$R\cos\theta,\ Z,\ R\sin\theta,\ BY,\ BZ,\ BX$$

with θ varying first, R varying second in that list. Z is the vertical direction (normal to the map mesh), $Z \equiv 0$.

1.b - Compute trajectories: for one turn, track a few protons on concentric trajectories centered on the center of the field map, ranging in $10 \leq R \leq 80\,\mathrm{cm}$ (radius R and particle momentum $p = qB\rho$ shall have proper correlation for that, to be determined). Plot these concentric trajectories in the a lab frame.

1.c - Plot the revolution time T_{rev} as a function of radius R and kinetic energy E_k (two abscissa axes). Superimpose the theoretical $T_{rev}(R)$ and $T_{rev}(E_k)$ curves. Explain what causes the slow increase of revolution period with energy. •

It is not possible to accelerate a particle traveling on a closed path using an electrostatic field $\tilde{E} = -\tilde{\mathrm{grad}}V(\tilde{R}, t)$ as the work by $\vec{F} = q\vec{E}$ only

depends on the initial and final states, it does not dependent on the path followed (Fig. 1.8):

$$\mathrm{W} = \int_{\mathrm{A}}^{\mathrm{B}} \vec{F}.d\vec{s} = -\mathrm{q}\int_{\mathrm{A}}^{\mathrm{B}} \vec{\mathrm{grad}}V.d\vec{s} = -\mathrm{q}(\mathrm{V_B} - \mathrm{V_A}).$$
$$\text{On a closed path : } \oint \vec{F}.d\vec{s} = 0 \qquad (1.1)$$

Instead, the work of a force of induction origin (the electric field arises

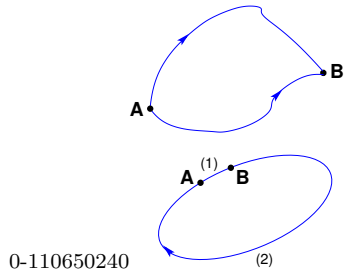

0-110650240

Fig. 1.8 The work of the electrostatic force only depends on V_A and V_B, independent of the path. In the case of the closed path: the particle loses along (2) the energy gained along (1).

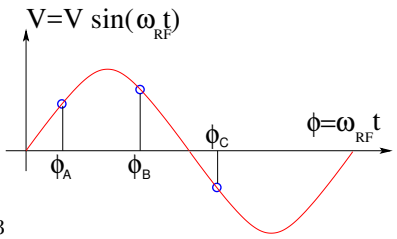

0100877673

Fig. 1.9 A particle which reaches the gap at $\omega_{\mathrm{RF}}\mathrm{t} = \phi_{\mathrm{A}}$ or $\omega_{RF}t = \phi_B$ is accelerated. If it reaches the RF gap at $\omega_{\mathrm{RF}}\mathrm{t} = \phi_{\mathrm{C}}$ it is decelerated.

from the variation of a magnetic flux, $\vec{E} = -\partial\vec{A}/\partial t$, $\vec{A}$ a vector potential) may not be null on a closed path. This is achieved *for instance* using a radio-frequency system which feeds an oscillating voltage across a gap, $\hat{\mathrm{V}}\sin(\omega_{\mathrm{RF}}\mathrm{t} + \phi)$ (Fig. 1.9). In the classical cyclotron the gap is formed mechanically by a double dee system (Fig. 1.5). In the separated sector cyclotron (Fig. 1.2) the accelerating system is an external resonant cavity inserted in the drift space between two magnets (in a similar manner as today's synchrotrons).

The quantities of concern, regarding orbital motion (R, $\mathrm{f_{rev}} = \omega_{\mathrm{rev}}/2\pi$), field (B), satisfy

$$\mathrm{BR} = \mathrm{p/q}, \qquad 2\pi\mathrm{f_{rev}} = \mathrm{v/R} = \mathrm{qB/m} \qquad (1.2)$$

These relationships hold whatever γ, from $v \ll c$ ($\gamma \approx 1$, domain of the *classical* cyclotron technology) to $\gamma > 1$ (domain of the *isochronous* cyclotron technology).

Note the first quantity introduced above, the *rigidity* of the particle of charge q and momentum p, BR = p/q, with R the curvature radius of the trajectory under the effect of the Laplace force in the field B. The *particle*

rigidity is a quantity of predilection in accelerator physics and design, it will be omnipresent along these lectures.

The RF frequency $f_{RF} = \omega_{RF}/2\pi$ is constant in a cyclotron. In the isochronous cyclotron it satisfies $f_{RF} = hf_{rev}$ at a great accuracy, at all time (Sec. 1.3.3). In the classical cyclotron f_{RF} is set, by design, equal to hf_{rev} for an intermediate energy during the acceleration cycle, as the revolution time does vary (decreases) (Sec. 1.2.4).

The energy gain, or loss, by the particle when transiting the gap is

$$\Delta W = q\hat{V}\sin\phi(t) \quad \text{with } \phi(t) = \omega_{RF}t - \omega_{rev}t + \phi_0 \tag{1.3}$$

with ϕ its phase with respect to the RF signal at the gap (*e.g.*, ϕ_A, ϕ_B or ϕ_C in Fig. 1.9) and ϕ_0 the value at $t = 0$, $\omega_{rev}t$ the orbital angle of the particle.

• **Exercise 1.1-2.** *Modeling an accelerating gap, acceleration in a cyclotron.*
Using the earlier 180 degree field map and zgoubi input file, introduce an accelerating gap with peak voltage 100 kV: simulate it by means of `CAVITE[IOPT=3]`, and reproducing the configuration of Fig. 1.6.
2.a - Inject a proton with starting kinetic energy 20 keV (at the appropriate starting radius, $R_0 = p_0/qB$, to be determined). Let it accelerate turn-by-turn through the gap (for multiturn, use `REBELOTE[NPASS=as many turns as needed; K=99]`, placed at the end of the sequence) until it reaches 6 MeV kinetic energy about. Plot the accelerated (spiraling out) trajectory all the way in a similar (O, X, Y) frame as in Fig. 1.7 (step-by-step particle data can be read from zgoubi.plt).
2.b - Plot the proton momentum pc and total energy E as a function of its kinetic energy, both from this numerical experiment (ray-tracing data stored using `FAISTORE`) and from theory, everything on the same graph, use MeV units.
2.c - Plot the normalized velocity $\beta = v/c$ as a function of kinetic energy, both numerical and theoretical, and in the latter case both classical and relativistic. •

• **Exercise 1.1-3.** *Accelerating to high energy: relativistic effects.*
Push the previous exercise to 3 GeV kinetic energy. For that, it will be necessary to extend the field map, to an maximum radius proper to encompass the spiraling trajectory up to 3 GeV. •

1.2 Classical cyclotron

Fixed-frequency acceleration requires matching between the RF and cyclotron frequencies. However the relativistic increase of the mass causes the revolution period to decrease with momentum, at a turn-by-turn rate of $\Delta T/T_{rev} = \gamma - 1$.

• **Exercise.** Give a theoretical demonstration of that relationship. •

The mis-match between the accelerating and cyclotron frequencies is a turn-by-turn cumulative effect and sets a limit to the highest velocity, $\beta = v/c \approx 0.22$, $\Delta T/T_{rev} \approx 2 - 3\%$. This will be addressed in Sec. 1.2.4. TFor the time being: this means for instance a limit of applicability of the "classical cyclotron" in the region $E - mc^2 \lesssim 25$ MeV for protons, $\lesssim 50$ MeV for D and α particles.

1.2.1 *Fixed-energy orbits, revolution period*

A common method for realistic modeling of the magnetic field of a cyclotron is to use a field map. Using a mathematical model is also a reasonable approach in a preliminary design phase due to the flexibility it brings in possibly tweaking parameters as for instance field homogeneity, radial or azimuthal field dependence. These two techniques are employed in the exercises to come.

• **Exercise 1.2.1-1.** *Numerical convergence of the integration method: field model and integration step size.*
********** j'en suis ici des "solutions" **********
1.2.1-1.a - In view of the next exercises, we will use from now on a 60 degree sector field map (the fortran program in App. 1.5.1 can be used again, *mutatis mutandis*). Check the evolution of orbit radius and revolution period with field map mesh density, namely:

- compute a field map with the density used in Ex. 1.1: radial increment of the mesh $\Delta R = 0.5$ cm, axial increment $\Delta\theta = 0.5$ cm/RM.;

- compute a second one with increments twice as large;

- plot the orbit radius R and revolution time T_{rev} as a function of the kinetic energ E_k in both cases, superpose the theoretical curves.

With the first map (denser mesh, more accurate field modeling) check the effect of the integration step size on these quantities.

1.2.1-1.b - Use instead Zgoubi's `DIPOLE` semi-analytical modeling for the field, and re-do the step-size test above.

Note : The optical sequence for this exercise is given in appendix 1.5.2.

1.2.1-1.c - From the two series of results, comment on various pros and cons of the two methods, analytical field models and field maps. •

• Exercise 1.2.1-2: cyclotron extraction and limitation in energy.
It follows from $qBR = p = \sqrt{2mW}$ (in the classical approximation, and with W the kinetic energy) that $\frac{\Delta R}{R} = \frac{1}{2}\frac{\Delta W}{W}$. with ΔW the energy gain per turn, this yields $\Delta R = \frac{m\Delta W}{q^2B^2R}$: the radius increment ΔR decreases with R. As the extraction at the last turn requires sufficient separation from the last but one for insertion of a deflector electrode (Fig. 1.5), there is a practical feasibility limit. Plot the accelerated spiral, or the fixed-energy orbits, to top energy, observe this property. Plot dR(R), from both tracking and theory. •

Periodic motion - Horizontal motion in a uniform field cyclotron has no privileged reference orbit: for a given momentum, the initial radius and velocity vector define a particular closed, circular orbit. A particle launched with an axial velocity component on the other hand, drifts vertically linearly with time, as there is no axial restoring strength component. The next Section will investigate the necessary field property, absent in our present field model so far, proper to ensure confinement of the multiturn periodic motion in the vicinity of the median plane of the cyclotron dipole magnet.
• Exercise 1.2.1-3. Observe the two statements above.
3.a - First statement: plot trajectories of particles launched with different initial velocity vector (zero axial component) over one turn. Give their theoretical parametric equation in a Cartesian frame (O;X,Y) centered at the center O of the cyclotron; supoerimpose with numerical trajectories (the option `IL=2` in `TOSCA` can be used to store particle coordinates through the field maps step-by-step).
3.b - Second statement: plot the axial motion of a particle launched with a non-zero initial axial velocity component. Give its theoretical vertical position Z(s) (Z is along the Lab. vertical axis, s is the path length); supoerimpose with the numerical trajectory. •

• Exercise 1.2.1-4. Unstable motion in uniform field.
4.a - Plot two particle trajectories that demonstrate the value of the radial wave number in a uniform field. Conclude on the orbit and on horizontal motion stability.
4.b - Derive the horizontal and axial transport matrices from ray-tracing (use `MATRIX[IFOC=11]`, placed in sequence with the optical sequence). Conclude on the stability of charged particle motion in a uniform field. •

1.2.2 *Weak focusing*

Let $B_r(r)$, $B_y(r)$ be respectively the radial and axial components of the magnetic field at a small radial displacement ($x = r - R, y$) from the reference circular orbit at R (centered at the center of the axially symmetric cyclotron magnet, Fig. 1.10). Assume median-plane symmetry of the field so that $B_r|_{y=0} = 0$ at all r (Fig. 1.10).

• Exercise. Demonstrate that the mid-plane symmetry hypothesis yields $B_r|_{y=0} = 0$. •

The radial and axial forces experienced by a particle at r, where the curvature radius is $r = R + x$, write, to the first order in the radial and axial coordinates, respectively x and y,

$$F_x = m\ddot{x} = -qvB_y(r) + m\frac{v^2}{R+x} \approx -qv(B_y(R) + \left.\frac{\partial B_y}{\partial r}\right|_R x) + m\frac{v^2}{R}(1 - \frac{x}{R})$$
$$F_y = m\ddot{y} = qvB_r(r) = qv \left.\frac{\partial B_r}{\partial y}\right|_{y=0} y + \text{higher order} \approx qv\frac{\partial B_y}{\partial r}y \qquad (1.4)$$

Note the following two steps in deriving these experessions:
- the force F_x which applies on the ion is the resultant of the pseudo force $f_c = m\frac{v^2}{r}$, oriented away from the center of the motion, and of the magnetic force $f_B = -qvB_y(r)$, oriented toward the center of the motion. In particular, $-qvB_y(R) + m\frac{v^2}{R} = 0$.
- a Taylor expansion of the magnetic field yields a first order expression of the r-dependence,

$$B_y(R+x) = B_y(R) + x \left.\frac{\partial B_y}{\partial r}\right|_R + \frac{x^2}{2!}\left.\frac{\partial^2 B_y}{\partial r^2}\right|_R + ... \approx B_y(R) + x \left.\frac{\partial B_y}{\partial r}\right|_R$$

The relations Eq. 1.4 yield the differential equations for the radial and axial motions, respectively,

$$\ddot{x} + \omega_r^2 x = 0 \qquad \text{and} \qquad \ddot{y} - \omega_y^2 y = 0 \qquad (1.5)$$

wherein $\omega_r^2 = \omega_{rev}^2(1 + \frac{R}{B}\frac{\partial B_y}{\partial r})$, $\omega_y^2 = \omega_{rev}^2 \frac{R}{B}\frac{\partial B_y}{\partial r}$, with $\omega_{rev} = 2\pi f_{rev}$ the angular frequency of the circular motion. Focusing by a restoring force appears (Eq. 1.5) owing to the use of a magnetic field with radial index

$$k(R) = \frac{R}{B}\frac{\partial B_y}{\partial r}|_{r=R,y=0} \qquad (1.6)$$

Radial stability in an axially symmetric structure with weakly decreasing field B(r) is sketched in Fig. 1.10-left : At larger motion radius, $r > R$

(resp. smaller, $r < R$), a particle with momentum $p = mv$ (assumed positively charged) experiences a decrease (resp. increase) of the outward force $f_c = m\frac{v^2}{r}$ at a higher rate than the decrease (resp. increase) of the bending force $f_B = -qvB$. In other words, radial stability requires BR to be an increasing function of R, $\frac{\partial BR}{\partial R} = B + R\frac{\partial B}{\partial R} > 0$ or $1 + k > 0$.

Axial stability imposes a guiding field decreasing with radius, Fig. 1.10-right, *i.e.*, $k < 0$, this ensures a restoring force directed toward the median plane.

The resulting condition of motion stability around the equilibrium orbit

$$-1 < k < 0 \tag{1.7}$$

is known as "weak focusing".

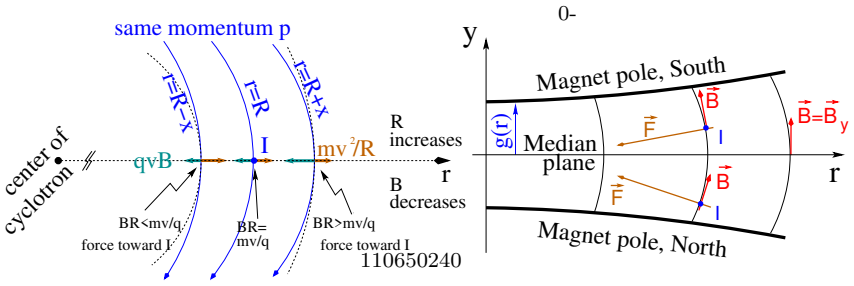

Fig. 1.10 Motion stability in a weak focusing axially symmetric structure. Left, radial: the resultant of the bending and outward forces pulls particles with momentum $p = mv$ toward the equilibrium orbit at $R = p/qB$, resulting in a stable oscillation around the latter. Right, axial: positive ions off the median plane (at I, coming out of the page) experience a force pulling toward the median plane. Note the hyperbolic shape of the gap $g(r) = g_0(r_0/r)^k$, creating the field $B(r) = B_0(r/r_0)^k$, Eq. 1.9.

The two quantities

$$\nu_r = \omega_r/\omega_{rev} = \sqrt{1+k}, \qquad \nu_y = \omega_y/\omega_{rev} = \sqrt{-k} \tag{1.8}$$

are known as, respectively, the radial and axial "wave number", the number of oscillations of the particle about the reference circular orbit of radius R. It can be seen that $\nu_r^2 + \nu_y^2$ takes it value on the unit radius circle in the wave number diagram (ν_r, ν_y).

Field profile - Keeping the focusing constant ($k = $ Const.) throughout the radial beam excursion requires an hyperbolic field profile: from Eq. 1.9 (and noting $B \equiv B_y$, assuming B only changes radially, introducing the field value B_0 at some reference radius R_0),

$$k = \frac{R}{B}\frac{dB}{dR} \Rightarrow \ln\frac{dB}{B} = k\ln\frac{dR}{R} \Rightarrow \frac{B}{B_0} = \left(\frac{R}{R_0}\right)^k \tag{1.9}$$

and B has to decrease with R, following a parabolic dependence, in order to ensure vertical focusing, so $k < 0$. This means in particular that the dipole gap has a parabolic shape, increasing with R (as $k < 0$), as sketched in Fig. 1.10.

Note in passing: scaling FFAG optics uses strong focusing instead, $k > 1$ and even $k \gg 1$, the gap (field) decreases (increases) rapidly with r, as a consequnce scaling FFAG optics is in general (*i.e.*, except for specific constraints on the momentum compaction) non-isochronous, this is treated in the FFAG Chapter.

• Exercise 1.2.2-1. Introducing a radial field index in a field map.
Use `TOSCA` and the field map method of exercise 1.2.1-1, construct the sector field map accounting for the radial index dependence $B(R) = B_0\,(R/R_0)^k$, $-1 < k \equiv$ constant < 0.
1.a - First, track a few tens of particles with momenta covering the radial extent of the field map, in order to check the k-dependence of B(R) (hint: match the numerical B(R) form the tracking, with the theoretical k-dependence above).
1.b - Plot the radial and axial paraxial motions of a 3 MeV ion over a few turns (using as earlier, `IL=2` under `TOSCA` and data thus stored in zgoubi.plt). Compare the trajectories for a few different index values, including close to 1 or close to 0.
1.c - Plot the energy dependence of the reference orbit radius, R(E).
1.d - Plot the R-dependence of the revolution period T_{rev} for the magnet with field index, from both ray-tracing (`FAISTORE` storage command can be used) and theory. •

Considering R_0 as a reference radius, with $B(R_0) = B_0$, and introducing the radial displacement $x = R - R_0$, Eq. 1.9 yields the following Taylor expansion,

$$\frac{B(R)}{B_0} = (1+\frac{x}{R_0})^k = 1+k\frac{x}{R_0}+\frac{k(k-1)}{2!}\left(\frac{x}{R_0}\right)^2+\frac{k(k-1)(k-3)}{3!}\left(\frac{x}{R_0}\right)^3+... \tag{1.10}$$

Now, identifying with the Taylor expansion as used in zgoubi's `DIPOLE` model, namely,

$$B(R_0+x) = B_0 + x\left.\frac{\partial B}{\partial R}\right|_{R_0} + \frac{x^2}{2!}\left.\frac{\partial^2 B}{\partial R^2}\right|_{R_0} + ... \tag{1.11}$$

one gets a possible Taylor-expansion approximation of the radial dependence of the vertical field component in the median plane of a weak-index

sector dipole, using the indices and derivatives series

$$\left.\frac{\partial B}{\partial R}\right|_{R_0} = k\frac{B_0}{R_0} \text{ (not surprisingly)}, \quad \left.\frac{\partial^2 B}{\partial R^2}\right|_{R_0} = k(k-1)\frac{B_0}{R_0^2}, \quad \text{etc.}$$

Note that the resulting first order approximation $B(R_0+x) \approx B_0(1+k\,x/R_0)$ makes the field index an R_0 dependent quantity, $k \equiv k(R_0)$: the practical value of k depends on the choice for R_0 (an arbitrary choice).

• Exercise 1.2.2-2. Introduce a radial field index, using the analytical modeling `DIPOLE`.
Repeat questions a to d of exercise 1.2.2-1. •

• Exercise 1.2.2-3. Introduce a radial field index, using the analytical modeling `FFAG`.
The `FFAG` element in zgoubi allows rigorous simulation the radial field dependence of Eq.1.9. Repeat questions a to d of exercise 1.2.2-1. •

• Exercise 1.2.2-4. Wave numbers in a weak focusing dipole magnet.
Use either the field map model of exercise 1.2.2-1, or the analytical models `DIPOLE` or `FFAG` of respectively exercises 1.2.2-2, 3, in order to simulate a dipole magnet with field index.
4.a - Compute the R-dependence of the radial and axial wave numbers ν_r and ν_y of the circular motion, using 1-turn mapping (use `MATRIX` to get the tunes, `FIT` to get the closed orbit for a particular momentum, and `REBELOTE` to scan a momentum range).
4.b - An alternate method: use `REBELOTE` for multi-turn raytracing of paraxial motion at constant energy (a few hundred turns is sufficient), for a series of different energies (one particle per energy) spanning the R range of interest. Log the turn-by-trun coordinates using `FAISTORE`, develop you own Fourier analysis tool, to be applied on the latter.
4.c - Show that $\nu_r^2 + \nu_y^2 = 1$, at all radius.
4.d - Compare the outcomes from the rigorous model `FFAG` for Eq. 1.9, and from the first order approximation of Eq. 1.11 using `DIPOLE`. •

Isochronism - The focusing condition $-1 < k < 0$ breaks the isochronism as it causes the guiding field B and thus $\omega_{rev} = qB/m$ to change (decrease) with R. As a consequence, the arrival time of a particle at the RF gap (by extension the "RF phase" of the motion) is not constant (this is addressed in Sec. 1.2.4).

1.2.3 *Coordinate transport*

Introducing the path variable, s, as the independent variable in Eq. 1.5, using the approximation ds ≈ vdt (and introducing a reference curvature radius ρ_0 in lieu of R, and the notation n = −k for the index, with 0 < n < 1), yields

$$\frac{\mathrm{d}^2\mathrm{x}}{\mathrm{ds}^2}+\frac{1-\mathrm{n}}{\rho_0^2}\mathrm{x}=0, \qquad \frac{\mathrm{d}^2\mathrm{y}}{\mathrm{ds}^2}+\frac{\mathrm{n}}{\rho_0^2}\mathrm{y}=0 \tag{1.12}$$

The solutions write, for respectively the horizontal and vertical motions,

$$\begin{cases} \mathrm{x(s)}=\mathrm{x_0}\cos\frac{\sqrt{1-\mathrm{n}}}{\rho_0}(\mathrm{s}-\mathrm{s_0})+\mathrm{x'_0}\frac{\rho_0}{\sqrt{1-\mathrm{n}}}\sin\frac{\sqrt{1-\mathrm{n}}}{\rho_0}(\mathrm{s}-\mathrm{s_0}) \\ \mathrm{x'(s)}=-\mathrm{x_0}\frac{\sqrt{1-\mathrm{n}}}{\rho_0}\sin\frac{\sqrt{1-\mathrm{n}}}{\rho_0}(\mathrm{s}-\mathrm{s_0})+\mathrm{x'_0}\cos\frac{\sqrt{1-\mathrm{n}}}{\rho_0}(\mathrm{s}-\mathrm{s_0}) \end{cases} \tag{1.13}$$

$$\begin{cases} \mathrm{y(s)}=\mathrm{y_0}\cos\frac{\sqrt{\mathrm{n}}}{\rho_0}(\mathrm{s}-\mathrm{s_0})+\mathrm{y'_0}\frac{\rho_0}{\sqrt{\mathrm{n}}}\sin\frac{\sqrt{\mathrm{n}}}{\rho_0}(\mathrm{s}-\mathrm{s_0}) \\ \mathrm{y'(s)}=-\mathrm{y_0}\frac{\sqrt{\mathrm{n}}}{\rho_0}\sin\frac{\sqrt{\mathrm{n}}}{\rho_0}(\mathrm{s}-\mathrm{s_0})+\mathrm{y'_0}\cos\frac{\sqrt{\mathrm{n}}}{\rho_0}(\mathrm{s}-\mathrm{s_0}) \end{cases} \tag{1.14}$$

• Exercise 1.2.3-1. Plot the horizontal and vertical coordinates of a particle trajectory, over 2-3 turns in the cyclotron. Verify that they satisfy Eqs. 1.13, 1.14 (use the option `IL=2` to store particle coordinates in zgoubi.plt, step-by-step). •

Note that the dissymmetry between the conditions of horizontal stability (n < 1 and the "1" term in "$\sqrt{1-\mathrm{n}}$") and vertical stability (0 < n, "$\sqrt{\mathrm{n}}$" instead) arises from the focusing introduced by the curvature, this is a purely geometrical effect. The associated focal distance to the curvature of a magnet of arc length $\mathcal{L}$ is obtained by integrating $\frac{\mathrm{d}^2\mathrm{x}}{\mathrm{ds}^2}+\frac{1}{\rho_0^2}\mathrm{x}=0$ and identifying with the focusing property $\Delta x' = -x/f$, namely,

$$\Delta\mathrm{x'}=\int\frac{\mathrm{d}^2\mathrm{x}}{\mathrm{ds}^2}\mathrm{ds}\approx\frac{-\mathrm{x}}{\rho^2}\int\mathrm{ds}=\frac{-\mathrm{x}\mathcal{L}}{\rho^2}, \quad \text{thus} \quad \mathrm{f}=\frac{\rho^2}{\mathcal{L}}$$

Chromatism, chromatic orbit - In an axially symmetric structure, the equilibrium trajectory at momentum $\begin{cases}\mathrm{p_0}\\ \mathrm{p_A}\end{cases}$ is at radius $\begin{cases}\rho_0 \text{ such that } \mathrm{B_0}\rho_0=\mathrm{p_0/q}\\ \rho_\mathrm{A} \text{ such that } \mathrm{B_A}\rho_\mathrm{A}=\mathrm{p_A/q}\end{cases}$, with $\begin{cases}\mathrm{B_A}=\mathrm{B_0}+\left(\frac{\partial\mathrm{B}}{\partial\mathrm{x}}\right)_0+...\\ \rho_\mathrm{A}=\rho_0+\Delta\mathrm{x}\\ \mathrm{p_A}=\mathrm{p_0}+\Delta\mathrm{p},\end{cases}$ On the other hand

$$\mathrm{B_A}\rho_\mathrm{A}=\frac{\mathrm{p_A}}{\mathrm{q}}\Rightarrow\left[\mathrm{B_0}+\left(\frac{\partial\mathrm{B}}{\partial\mathrm{x}}\right)_0\Delta\mathrm{x}+...\right][\rho_0+\Delta\mathrm{x}]=\frac{\mathrm{p_0}+\Delta\mathrm{p}}{\mathrm{q}}=\frac{\mathrm{p_0}}{\mathrm{q}}+\frac{\Delta\mathrm{p}}{\mathrm{q}}$$

and, neglecting terms in $(\Delta x)^2$: $B_0\rho_0 + \left(\frac{\partial B}{\partial x}\right)_0 \rho_0 \Delta x + B_0 \Delta x = \frac{p_0}{q} + \frac{\Delta p}{q}$, which, given $B_0\rho_0 = \frac{p_0}{q}$, leaves $\Delta x \left[\left(\frac{\partial B}{\partial x}\right)_0 \rho_0 + B_0\right] = \frac{\Delta p}{q}$, which given $n = -\frac{\rho_0}{B_0}\left(\frac{\partial B}{\partial x}\right)_0$ yields

$$\Delta x = \frac{\rho_0}{1-n}\frac{\Delta p}{p_0} = D\frac{\Delta p}{p_0} \tag{1.15}$$

In passing we have introduced the quantity $D = \frac{\rho_0}{1-n}$, the "dispersion"

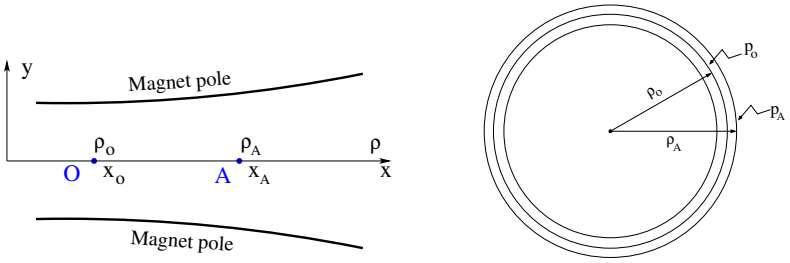

Fig. 1.11 The equilibrium radius at location $O(x = x_0)$ is $\rho = \rho_0$, the equilibrium momentum is p_0, rigidity $B\rho = B_0\rho_0$. The equilibrium radius at $A(x = x_A)$ is $\rho = \rho_A$ for the particle with momentum $p_A = p_0 + \Delta p$, rigidity $B\rho = B_A\rho_A$.

factor with respect to the reference closed orbit at ρ_0. This establishes that D(s) is the solution of the differential equation

$$\frac{d^2D}{ds^2} + \frac{1-n}{\rho_0^2}D = \frac{1}{\rho_0} \tag{1.16}$$

and is a constant in the present case of the cylindrical-symmetry cyclotron structure.

Momentum compaction - A chromatic closed orbit $x(s) = D\frac{\Delta p}{p}$ has a different length, $\mathcal{L}+\delta\mathcal{L}$, with $\mathcal{L}$ the length of the "on-momentum" closed orbit. The trajectory lengthening, or "momentum compaction" compaction, is

$$\alpha = \frac{\Delta\mathcal{L}/\mathcal{L}}{\Delta p/p} = \frac{\Delta R/R}{\Delta p/p} = \frac{1}{(1-n)} = \frac{1}{\nu_x^2} \tag{1.17}$$

with the rightmost expression by virtue of Eq. 1.8.

• Exercise 1.2.3-2. In the optical conditions of Ex. 1.2.3-1,
2.a - check the trajectory lengthening of "chromatic orbits", Eq. 1.17 , plot it as a function of $\Delta p/p$,
2.b - based on Fourier analysis of particle motion, check $\alpha = \frac{1}{\nu_x^2}$, Eq. 1.17 ,
2.c - plot the dispersion term around the ring D(s), check that it does not depend on s •

Betatron wavelength - Introducing $\theta = \mathrm{s}/\rho$ as the independent variable Eq. 1.12 becomes

$$\frac{\mathrm{d}^2\mathrm{z}}{\mathrm{d}\theta^2} + \nu^2\mathrm{z} = 0, \quad \begin{cases} \text{radial motion}: \quad \mathrm{z} = \mathrm{x} \text{ and } \nu = \nu_\mathrm{x} = \sqrt{1-\mathrm{n}} \\ \text{vertical motion}: \mathrm{z} = \mathrm{y} \text{ and } \nu = \nu_\mathrm{y} = \sqrt{\mathrm{n}} \end{cases} \tag{1.18}$$

This is the differential equation of the harmonic oscillator, with solution (that can also be inferred from Eqs. 1.13, 1.14)

$$\mathrm{z} = \mathrm{z}_0 \cos\nu\theta + \frac{\mathrm{z}'_0}{\nu}\sin\nu\theta, \quad \frac{\mathrm{dz}}{\mathrm{d}\theta} = -\nu\mathrm{z}_0 \sin\nu\theta + \mathrm{z}'_0 \cos\nu\theta \tag{1.19}$$

This can be written in the alternate form

$$\mathrm{z} = \hat{\mathrm{z}}\cos(\nu\theta + \phi), \quad \frac{\mathrm{dz}}{\mathrm{d}\theta} = -\nu\hat{\mathrm{z}}\sin(\nu\theta + \phi) \tag{1.20}$$

where,

$$\hat{\mathrm{z}} = \sqrt{\mathrm{y}_0^2 + \frac{\mathrm{y}'^2_0}{\nu^2}}, \quad \phi = -\mathrm{atan}\frac{\mathrm{y}'_0}{\nu\mathrm{y}_0} \tag{1.21}$$

The consequence is $\hat{z}^2 = y_0^2 + \frac{y'^2_0}{\nu^2} = y^2 + \frac{y'^2}{\nu^2}$: $\hat{z}$ is an invariant of the motion.

• Exercise 1.2.3-3. Track a particle with small amplitude radial and axial motions, at constant energy, in a ring cyclotron based on the earlier material.
3.a - Plot $\mathrm{x}(\theta)$, $\mathrm{y}(\theta)$ around the ring over 3-4 turns. Check that the observed fraction of wavelength per turn (radial or axial), identifies with the wave number (hint: use a fitting procedure to match the trajectory with the expected Eqs. 1.13, 1.14). Check against theoretical expectation.
3.b - Record particle coordinates x, y at some fixed azimuth s around the ring, compute its radial and axial wave numbers by Fourier analysis. What is the indetermination on the wave number? Explain.
3.c - At some azimuth s around the ring, observe the particle coordinates as it circles around, plot them (in both cases z = x, z = y) in a $(\mathrm{z}, \frac{1}{\nu_\mathrm{z}}\frac{\mathrm{dz}}{\mathrm{d}\theta})$ diagram. What is the form of the trajectory in this representation? In what direction, clockwise or counterclockwise, is the particle moving? •

1.2.4 *Resonant acceleration*

An oscillating radio-frequency (RF) electric field, with fixed-frequency $\mathrm{f_{RF}}$ is applied in the gap between the two dees (Fig. 1.5). An ion of charge q reaching the gap at time t undergoes a change in energy

$$\Delta\mathrm{W(t)} = \mathrm{q}\hat{\mathrm{V}}\sin\phi \quad \text{with } \phi = \omega_\mathrm{RF}\mathrm{t} - (\omega_\mathrm{rev}\mathrm{t} + \phi_0) \tag{1.22}$$

with ϕ the RF phase experienced by the particle at the time it crosses the gap and ϕ_0 the origin in phase for the particle motion (normally about $\pi/2$, in the region of the crest of V(t) oscillation). Note that this ignores the "transit time", the effect of the time that the particle spends across the gap on the overall energy gain; focusing in the cyclotron, in what follows, will ignore as well the effect of the electric gap.

The frequency dependence of the kinetic energy W of the ion relates to its orbital radius R in the following way:

$$W = \frac{1}{2}mv^2 = \frac{1}{2}m(2\pi R f_{rev})^2 \approx \frac{1}{2}m(2\pi R\frac{f_{RF}}{h})^2 \qquad (1.23)$$

thus, for a given cyclotron size (R), f_{RF} and h set the limit for the acceleration range.

The revolution time/frequency increases/decreases with energy and the condition of synchronism with the oscillating voltage, $f_{RF} = hf_{rev}$, is only fulfilled at one particular radius in the course of acceleration (Fig. 1.12). To the left and to the right, out-phasing $\Delta\phi$ builds-up turn after turn, decreasing in a first stage (towards zero, $\phi < \pi/2$ and lower voltages, Fig. 1.12-right) and then increasing (back to the starting $\phi = \pi/2$ phase and beyond towards $\phi > \pi$, deceleration).

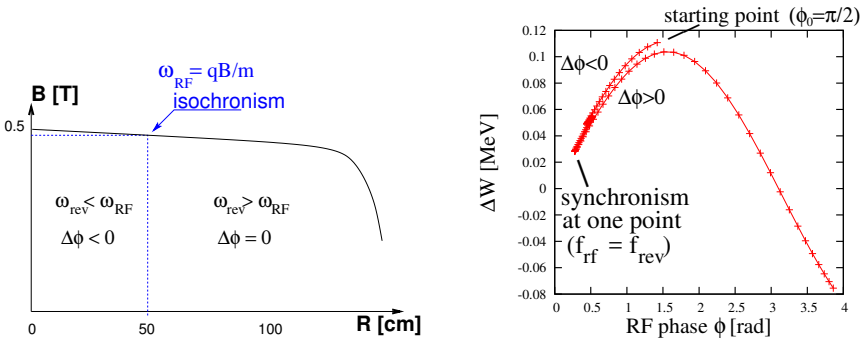

Fig. 1.12 Synchronous condition at one point (left), and span in phase of the accelerating voltage in $[0^o, > 180^o]$ range (right). ϕ is the arrival phase of the particle at the gap, *i.e.*, the phase of the RF sine voltage at the time the particle meets the gap. Note that the vertical separation of the two $\Delta W(\phi)$ branches on the right ($\Delta\phi < 0$ and $\Delta\phi > 0$) is artificial, this is for clarity, they are actually superimposed.

Differentiating the particle phase at the RF gap, over a half-turn (Eq. 1.22 with ω_{rev} constant between two gaps) one gets $\dot{\phi} = \omega_{RF} - \omega_{rev}$. Over a half-turn in addition, $\Delta\phi = \dot{\phi}\frac{\pi R}{v}$, yielding a phase-shift per half-turn

of

$$\Delta\phi = \pi\left(\frac{\mathrm{m}\omega_{\mathrm{RF}}}{\mathrm{qB}} - 1\right) \tag{1.24}$$

Due to this cumulative out-phasing the classical cyclotron requires quick acceleration (limited number of turns), which means high voltage (tens or hundreds of kVolts). As expected, with ω_{RF} and B constant, $\Delta\phi$ presents a minimum ($\dot{\phi} = 0$) at $\omega_{\mathrm{RF}} = \omega_{\mathrm{rev}} = \frac{\mathrm{qB}}{\mathrm{m}}$ where exact isochronism is reached (Fig. 1.12). The upper limit to ϕ is set by the condition $\Delta\mathrm{W} > 0$, acceleration.

• Exercise 1.2.4-1. Phase-shift at the accelerating gap.
Consider the weak focusing cyclotron of exercise 1.2.2-2, with a double accelerating gap. Take the following parameters: field index $\mathrm{n} = -0.03125$, field $\mathrm{B}_0 = 5\,\mathrm{kG}$ on injection radius, injection energy $\mathrm{W}_0 = 200\,\mathrm{keV}$, peak gap voltage $\hat{\mathrm{V}} = 100\,\mathrm{kV}$. Assume, first, that the acceleration is independent of the arrival phase (use `CAVITE[IOPT=3]`, at both gaps).
1.a - Track a proton from 1 to 5 MeV: get the turn-by-turn phase-shift at the gap, compare with Eq. 1.24.
1.b - Produce a similar diagram $\Delta\mathrm{W}(\phi)$ to Fig. 1.12-right. •

• Exercise 1.2.4-2. The cyclotron equation.
In the cyclotron conditions of exercise 1.2.4-1, set the isochronism at halfway of the radial extent of the cyclotron.
2.a - Give the volues of: the RF frequency, the energy at which isochronism is met.
2.b - Plot the theoretical energy-phase relationship characteristic of the cyclotron acceleration:

$$[\cos\phi](\mathrm{W}) = \cos\phi_0 + \pi\left[1 - \frac{\omega_{\mathrm{RF}}}{\omega_{\mathrm{rev0}}}(1 + \frac{\mathrm{W}}{2\mathrm{m}_0\mathrm{c}^2})\right]\frac{\mathrm{W}}{\mathrm{q}\hat{\mathrm{V}}} \tag{1.25}$$

for $\phi_0 = \frac{3\pi}{4},\ \frac{\pi}{2},\ \frac{\pi}{4}$.
2.c - Produce these curves numerically, superimpose on the same graph.•

1.3 Relativistic cyclotron

The bad news with relativistic energies, is, from the cyclotron resonance $\omega_0 = \mathrm{qB}/\gamma\mathrm{m}_0$, given $\mathrm{R} = \beta\mathrm{c}/\omega_0$, one gets

$$\mathrm{k} = \frac{\mathrm{R}}{\mathrm{B}}\frac{\partial\mathrm{B}}{\partial\mathrm{R}} = \frac{\beta}{\gamma}\frac{\partial\gamma}{\partial\beta} = \beta^2\gamma^2 \tag{1.26}$$

Thus k is positive and increases with energy: the weak focussing condition $-1 < k < 0$ is not satisfied.

• Exercise 1.3-1. In passing, demonstrate (or correct in case of an error) the following relationships:
$\frac{dp}{p} = \frac{1}{\beta^2}\frac{dE}{E}$; $\frac{d\beta}{\beta} = \frac{1}{\gamma^2}\frac{dp}{p} = \frac{1}{\beta^2\gamma^2}\frac{dE}{E}$; $\frac{d\gamma}{\gamma} = \frac{dW}{m_0+W}$ (W = kinetic energy); $\frac{dW}{W} = \frac{\gamma+1}{\gamma}\frac{dp}{p}$. •

The revolution period on the equilibrium orbit, momentum $p = qBR$ and circumference $\mathcal{C}$, is $T = \mathcal{C}/\beta c = 2\pi\gamma m_0/qB$. Isochronism requires p-invariant revolution period, $dT/dp = 0$. Differentiating the previous expression, this requirement yields

$$B(R) = \frac{B_0}{\gamma_0}\gamma(R) \tag{1.27}$$

with B_0 and γ_0 free reference conditions, and the reference revolution period is noted T_0. In other words, isochronism requires $B(R) \propto \gamma$, which happens to yield axial defocusing!

H.A. Bethe and M.E. Rose once stressed [3] "... it seems useless to build cyclotrons of larger proportions than the existing ones... an accelerating chamber of 37 cm radius will suffice to produce deuterons of 11 MeV energy which is the highest possible...". Frank Cole : "If you went to graduate school in the 1940s, this inequality $[-1 < k < 0]$ was the end of the discussion of accelerator theory."

Until...

1.3.1 *Thomas focusing*

In 1938, L.H. Thomas introduces the concept of alternating regions of stronger and weaker axial field [4], the "AVF" (Azimuthally Varying Field) cyclotron (Fig. 1.13). The single-magnet concept of the classical cyclotron remains, the azimuthal field modulation is obtained by shaping the magnet pole to create a $2\pi/N$-periodical field form factor, the "flutter", for instance with the undulating form

$$\mathcal{F}(\theta) \propto 1 + f\sin(N\theta) \tag{1.28}$$

The radial increase of the field (Eq. 1.27) for isochronism of the orbits is obtained by radial pole shaping. The median plane field now varies with both R and θ,

$$B(R,\theta) = B_0\,\mathcal{R}(R)\,\mathcal{F}(\theta) \tag{1.29}$$

This azimuthal variation of the field amplitude introduces an azimuthal component in the field index :

$$\mathrm{k} = \frac{\rho}{\mathrm{B}}\frac{\mathrm{dB}}{\mathrm{dx}} = \frac{\rho}{\mathrm{B}}\left[\frac{\partial \mathrm{B}}{\partial \mathrm{R}}\frac{\mathrm{dR}}{\mathrm{dx}} + \frac{\partial \mathrm{B}}{\partial \theta}\frac{\mathrm{d}\theta}{\mathrm{dx}}\right] \tag{1.30}$$

Note the introduction of a local curvature radius, $\rho(\mathrm{s})$, as the orbit curvature is no longer constant along the orbit as a consequence of the AVF.

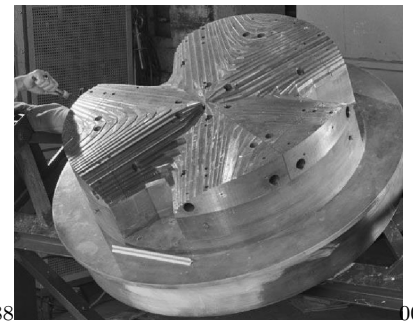
00956888

Fig. 1.13 Azimuthal pole shaping in Thomas-style AVF cyclotron.

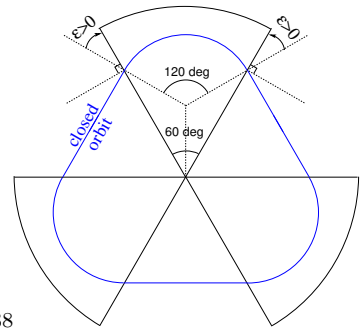

00956888

Fig. 1.14 Sketch of a 3-period AVF cyclotron, based on 120 degree sector dipoles. The dipole edges make a $\epsilon = 30$ degree "wedge angle". This is a "closing" of the magnet, it causes vertical focusing and weakens the horizontal focusing (*cf.* Fig. 1.16).

A sector dipole with index

We now introduce the transfer matrix of a sector magnet, pushing Thomas' modulation to the point that the field varies abruptly between 0 and B_0 at sector edges (a simplified, so-called "hard-edge", model of a sector dipole). Bending sections span a fraction of 2π and the "filling factor" (ratio of magnetic length to circumference along a closed orbit, $\mathrm{L_{mag}}/2\pi\mathrm{R}$) is < 1.

Eqs. 1.13 1.14) which express the transport of the coordinate of a particle as it propagates through the hard-edge bending sector, can be written under matrix form, namely

$$\begin{pmatrix} \mathrm{x} \\ \mathrm{x}' \\ \mathrm{y} \\ \mathrm{y}' \end{pmatrix}_{\mathrm{out}} = \begin{pmatrix} \cos\sqrt{k_x}\mathcal{L} & \frac{1}{\sqrt{k_x}}\sin\sqrt{k_x}\mathcal{L} & 0 & 0 \\ -\sqrt{k_x}\sin\sqrt{k_x}\mathcal{L} & \cos\sqrt{k_x}\mathcal{L} & 0 & 0 \\ 0 & 0 & \cos\sqrt{k_y}\mathcal{L} & \frac{1}{\sqrt{k_y}}\sin\sqrt{k_y}\mathcal{L} \\ 0 & 0 & -\sqrt{k_y}\sin\sqrt{k_y}\mathcal{L} & \cos\sqrt{k_y}\mathcal{L} \end{pmatrix} \begin{pmatrix} \mathrm{x} \\ \mathrm{x}' \\ \mathrm{y} \\ \mathrm{y}' \end{pmatrix}_{\mathrm{in}} \tag{1.31}$$

wherein "*in*" and "*out*" stand for the entrance ($s = s_{in}$) and exit ($s = s_{out}$) of the sector, $k_x = (1-n)/\rho^2$, $k_y = n/\rho^2$, $\mathcal{L}$ is the length of the arc of curvature ρ (which coincides with the trajectory of reference momentum $p = mv$ at radius R). The null anti-diagonal coefficients in this 4×4 matrix representation express the fact that the radial and axial components of the motion are independent, "*decoupled*". Obviously, the transport can be expressed for Eq. 1.13 and Eq. 1.14) independently, under the form of a 2×2 matrix relationship,

$$\begin{pmatrix} x \\ x' \end{pmatrix}_{out} = \begin{pmatrix} \cos\sqrt{k_x}\mathcal{L} & \frac{1}{\sqrt{k_x}}\sin\sqrt{k_x}\mathcal{L} \\ -\sqrt{k_x}\sin\sqrt{k_x}\mathcal{L} & \cos\sqrt{k_x}\mathcal{L} \end{pmatrix} \begin{pmatrix} x \\ x' \end{pmatrix}_{in} \tag{1.32}$$

$$\begin{pmatrix} y \\ y' \end{pmatrix}_{out} = \begin{pmatrix} \cos\sqrt{k_y}\mathcal{L} & \frac{1}{\sqrt{k_y}}\sin\sqrt{k_y}\mathcal{L} \\ -\sqrt{k_y}\sin\sqrt{k_y}\mathcal{L} & \cos\sqrt{k_y}\mathcal{L} \end{pmatrix} \begin{pmatrix} y \\ y' \end{pmatrix}_{in} \tag{1.33}$$

• Exercise 1.3.1-1. Compute the 4×4 transport matrix of a 60^o sector with index $0 < n < 1$ (say, $n = 0.6$) and curvature ρ for the reference momentum p (Fig. 1.15-left), from the ray-tracing of an appropriate set of rays. Compare with theory. •

• Exercise 1.3.1-2. The focal distance associated with the curvature (index $n = 0$, magnet length $\mathcal{L}$ and curvature radius ρ) satisfies

$$\frac{d^2x}{ds^2} + \frac{1}{\rho^2}x = 0 \Rightarrow \Delta x' = \int \frac{d^2x}{ds^2}ds \approx -\frac{x}{\rho^2}\int ds = -\frac{x}{\rho^2}\mathcal{L} \stackrel{\text{def.}}{\equiv} -\frac{x}{f} \Rightarrow f = \frac{\rho^2}{\mathcal{L}}$$

Verify the value of f in the case of a $\alpha = 60^o$ sector dipole with index n, by ray-tracing paraxial rays with incoming incidence zero and coordinates $\pm x$. •

• Exercise 1.3.1-3. The geometrical focusing in a constant field dipole (Fig. 1.15-right) stems from the longer (shorter) path in the magnetic field for rays entering the magnet at greater (smaller) radius.
3.a - Raytrace three rays with identical momentum, $p = qB\rho$, entering at respectively $R^- < R_0 < R^+$, through a $\alpha = 60^o$ sector dipole with zero field index. Show that the field integrals through the magnet satisfy $\int B\,ds/B\rho = \theta$, and thus $\theta^- < \theta_0 < \theta^+$.
3.b - This effect can be cancelled if particles at greater (smaller) radius find a smaller (greater) field: this would result in ΔB such that $\Delta x = OO' = 0$, $\Delta x = O''O = 0$, in Fig. 1.15. Differentiation of $B\rho = C^{st}$ yields $\frac{\Delta B}{B} + \frac{\Delta\rho}{\rho} = 0$, hence a required index $n = -\frac{\rho}{B}\frac{\Delta B}{\Delta x} = 1$. Verify that property by ray-tracing three parallel incoming rays of equal momenta. •

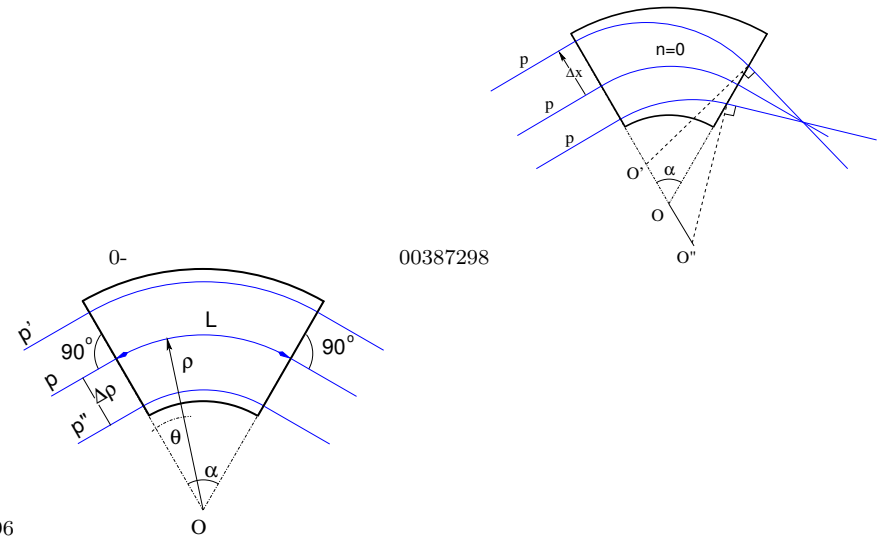

Fig. 1.15 Left: an $\alpha = 60^{o}$ sector dipole with index n. At constant radius, B is constant, a particle with *small* momentum deviation $\Delta p = q(1-n)B\Delta\rho$ will follow an arc of radius $\rho + \Delta\rho$. Right, case of field index n = 0: parallel incoming rays of equal momenta come out converging. Radial trajectory convergence (focusing) in a uniform field sector dipole is a purely geometrical property.

Wedge focusing

A historical note in passing: wedge focusing would eventually be the technique used for the ZGS, "Zero Gradient Synchrotron", a 12 GeV ring at Argonne. This will be addressed in the weak focusing synchrotron chapter. The interest is that it simplifies the sector magnet as it avoids profiling its poles (as $n = 0$).

The transport of the transverse (radial and axial) particle coordinates through a dipole magnet edge, with wedge angle ϵ can be written under the matrix form

$$\begin{pmatrix} x \\ x' \\ y \\ y' \end{pmatrix}_2 \begin{pmatrix} 1 & 0 & 0 & 0 \\ -\tan\frac{\epsilon}{\rho} & 1 & 0 & 0 \\ 0 & 0 & 1 & 0 \\ 0 & 0 & \tan\frac{\epsilon}{\rho} & 1 \end{pmatrix} \begin{pmatrix} x \\ x' \\ y \\ y' \end{pmatrix}_1 \tag{1.34}$$

The transport matrix of a dipole magnet with wedge angles ($\epsilon \neq 0$) writes

$$\mathrm{M} = \mathrm{W_o} \times \mathrm{M_{sector}} \times \mathrm{W_i} \tag{1.35}$$

with $\mathrm{W_o}$, exit wedge (respectively $\mathrm{W_i}$, entrance wedge) a matrix of the form Eq. 1.34 and M the sector matrix of Eq. 1.32.

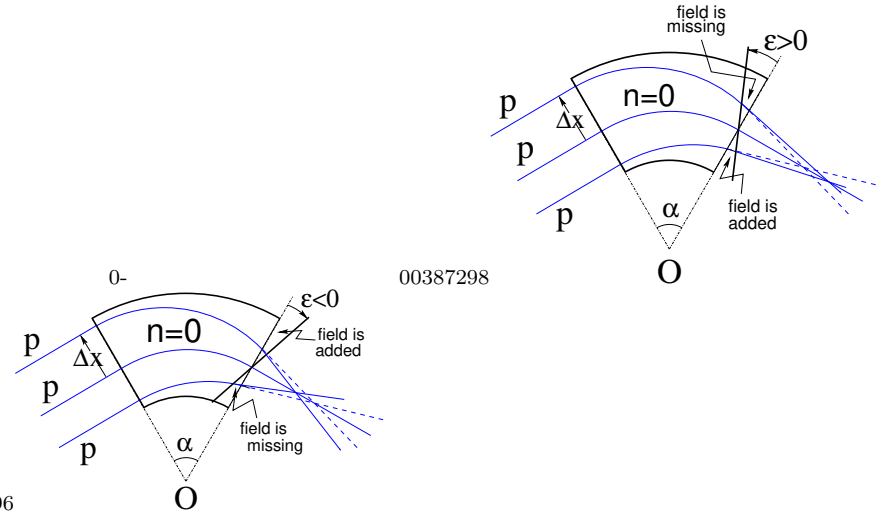

Fig. 1.16 Left: a focusing wedge ($\epsilon < 0$ by convention), opening the sector augments the horizontal focusing. Right: a defocusing wedge ($\epsilon > 0$ by convention), closing the sector diminishes the horizontal focusing. Focal distance in the bend plane respectively decreases, increases. The reverse holds in the vertical plane, opening/closing the sector decreases/increases the vertical focusing.

• Exercise 1.3.1-4. From ray-tracing, get the transport matrix of a 120° sector in the two cases of (i) no wedge angle, (ii) 30° wedge angle at entrance and exit as sketched in Fig. 1.14. Show that in the second case the dipole is both radially and axially focusing. Check against Eq. 1.34 . •

The "flutter" F characterizes the steepness of the azimuthal field fall-off $\mathcal{F}(\theta)$ over an extent λ at magnet ends. For a given orbit, of average radius $\mathrm{R} = \oint \mathrm{ds}/2\pi$ and of curvature $\rho(\mathrm{s})$ inside the dipole, it writes

$$\mathrm{F} = \left(\frac{< \mathcal{F}^2 > - < \mathcal{F} >^2}{< \mathcal{F} >^2} \right)^{1/2} \xrightarrow{\lambda \to 0} \frac{\mathrm{R}}{\rho} - 1 \tag{1.36}$$

with $\mathrm{F} = \frac{\mathrm{R}}{\rho} - 1$ the "hard-edge" field fall-off case, *i.e.*, the (unphysical) case when $\mathcal{F}(\theta)$ steps from 1 to 0 at the location of the magnet edge. Edge focussing permits the necessary $\mathrm{B(R)} \propto \gamma(\mathrm{R})$ (Eq. 1.27) as it ensures axial focusing. If the scalloping of the orbit is small, *i.e.*, if $\mathcal{C}/2\pi \approx \rho$ (*i.e.*, the presence of drifts only causes a small departure of the $\mathcal{C}$-circumference closed orbit from the average radius $\mathcal{C}/2\pi$), then

$$\nu_\mathrm{x} \approx \sqrt{1 - \mathrm{n}} \quad \text{and} \quad \nu_\mathrm{y} \approx \sqrt{\mathrm{n} + \mathrm{F}^2} \tag{1.37}$$

in a first approach. The flutter causes $n + F^2 > 0$ (whereas $n < 0$, B increases with R for isochronism) thus the vertical motion is stable in the sense of periodic stability (ν_y is real). Expectedly from what precedes, the fringe field modifies the first order vertical mapping, namely, the wedge focussing (Eq. 1.34) is changed in the following way:

$$R_{43=}\frac{\tan(\epsilon)}{\rho} \rightarrow R_{43} = \frac{\tan(\epsilon - \psi)}{\rho} \tag{1.38}$$

wherein

$$\psi = I_1 \frac{\lambda}{\rho}\frac{1+\sin^2\epsilon}{\cos\epsilon}, \quad \text{with } I_1 = \int_{s|_{B=0}}^{s|_{B=B_0}} \frac{B(s)(B_0 - B(s))}{B_0^2}\frac{ds}{\lambda} \tag{1.39}$$

with $B(s)$ the median-plane field, ϵ the wedge angle (Fig. 1.16), and the integral I_1 extends over the field fall-off where B evolves in the range $[0, B_0]$, B_0 being the field value reached inside the magnet. Horizontal focusing is only affected to second order in the (x, x') coordinates, the first order mapping of Eq. 1.34 is unchanged.

• Exercise 1.3.1-5. Play with the extent λ of the fringe field in the 120 degree sector dipole of Ex. 1.3.1-5: from extremely short (quasi hard-edge) to very long. Check the evolution of horizontal and vertical focusing of the magnet, and of the wave numbers of the ring. •

1.3.2 *Spiral sector*

In 1954 Kerst introduces a method for vertical wedge focusing which compensates for the radially increasing field gradient: by spiraling the edges of the sector dipoles (Fig. 1.3)

$$B(R,\theta) = B_0\,\mathcal{F}(R,\theta)\,\mathcal{R}(R), \quad \mathcal{F}(R,\theta) = 1 + f\sin(N(\theta - \tan(\xi)\ln(R/R_0))) \tag{1.40}$$

$R = R_0\exp(\theta/\tan(\xi))$ is the equation of the spiral, centered at the center of the ring. This results in a larger contribution of the flutter term in the vertical wave number,

$$\nu_z = \sqrt{n + F^2(1 + 2\tan^2\xi)} \tag{1.41}$$

with ξ the spiral angle: the angle that the tangent to the spiral edge does with the ring radius.

In the late 1950s appeared the "separated sector cyclotron", in which the sector dipoles are separated by iron-free (not really field-free, though, due

the the field fall-offs) spaces (Fig. 1.2). Isochronous cyclotrons nowadays still rely on these various principles and techniques, their limit in energy resides in achievable field strength, magnet size, and beam separation at the last turn for extraction.

An instance of a single-magnet spiral sector AVF cyclotron is PSI's 250 MeV protontherapy machine, Fig. 1.3, the field at the center of the cyclotron is 2.4 T. An instance of a separated spiral sector cyclotron is PSI's 590 MeV, Fig. 1.2. Simulations regarding fixed-field spiral sector optics are postponed to the FFAG chapter.

1.3.3 *Isochronous acceleration*

Data regarding PSI cyclotron (Fig. 1.2) are provided in a separate document, see CASE web page.

1.4 summary

During this laboratory work session, we have learned about the following:

- the uniform field (single-magnet) classical cyclotron, field characterized by B(θ) =constant, slowly decreasing with R for vertical stability of the motion,
- weak transverse focusing, in both planes simultaneously, defined by an hyperbolic radial dependence of the field, $B(R) = B_0 \frac{R_0}{R^\alpha}$ $(0 < \alpha < 1)$,
- near-crest loosely-isochronous resonant acceleration in the classical cyclotron, a low-energy machine,
- Thomas' isochronous single-magnet "AVF" cyclotron; azimuthal field modulation ("flutter") and vertical focusing, with for instance $B(\theta) \propto B_0(1 + f \sin(3\theta))$,
- wedge focusing, enhanced vertical wedge focusing by spiraling the pole edges,
- the isochronous cyclotron, a separated sector ring accelerator,
- isochronous resonant acceleration in PSI cyclotron.

Various notions and quantities proper to the characterization of charged particle dynamics in accelerators have been introduced, including:

- closed orbit,
- field index, focusing,
- differential equations of the motion, and their periodic solutions,
- betatron wavelength, motion invariant,
- dispersion function,

- transport of particle coordinates, dipole and wedge transport matrices.

1.5 Appendix

1.5.1 *Field map and optical sequence for Exercise 1.1-1*

The cyclotron is defined using a 180 degree field map twice. This optical sequence can be copy-pasted to a Zgoubi input data file and run as it is, once the magnetic field map has been built (and saved in "geneSectorMap.out").

Consult zgoubi users' guide for the functionning of the various keywords (`OBJET`, `PARTICUL`, `FAISTORE`, `TOSCA`, `FAISCEAU`, `END`) and their subsequent data list.

Fortran program that generates a field map

This program builds a 180 degree magnetic field map in the appropriate format for zgoubi's `TOSCA [IX=315,IY=121,IZ=1,MOD=22]` field map reading mode. Save it in "geneSectorMap_180deg.out" for this exercise.

```
      implicit double precision (a-h,o-z)
      parameter (pi = 4.d0*atan(1.d0))

C------------ Hypotheses: they allow building a field map for use by zgoubi's TOSCA
C keyword. See zgoubi users' gudie for the list of input data needed under TOSCA
C (these presnt values may change, depending on the exercise) :

C Total angle extent of the field map, AT (360 deg. here):
      AT = 180.d0  /180.d0*pi
C Radial extent of the field map
      Rmi = 10.d0   ! cm
      Rma = 70.d0   ! cm
C Take RM=50 cm reference radius, as this value (arbitray, taken
C to be about half-way from Rmi to Rma) is found in various exercises
      RM = 50.d0
C dX=RM*dA is the arc length between 2 nodes along R=RM arc, given angle increment dA
C A good starting point (by experience) is dX a few mm, say ~0.5 cm
      dX = 0.5d0  ! 0.5 cm mesh step at RM, allows getting NX=NINT(RM*AT/dX)+1
C dR is the radial distance between two nodes, good starting point is dR = 0.5 cm
      NR = 120 + 1               !!!!! TOSCA's 'IY'
C Finally, field :
      BZ = 5.d0  ! kG
C-----------------------------------------------

      dR = (Rma - Rmi) / (NR -1)

      NX = NINT(RM*AT / dX)  +1  !!!!! TOSCA's 'IX'
      dX = RM*AT / DBLE(NX - 1)  ! exact step length at RM, corresponding to NX
      dA = dX / RM               ! corresponding step in angle, delta_theta
      A1 = 0.d0 ; A2 = AT

      BY = 0.d0 ; BX = 0.d0 ; Z = 0.d0

      open(unit=2,file='geneSectorMap.out')
      write(2,*) Rmi,dR,dA/pi*180.d0,dZ,
     >'     !  Rmi/cm, dR/cm, dA/deg, dZ/cm'
      write(2,*) '# Field map generated using geneSectorMap.f '
      write(2,fmt='(a)') '# AT/rd,  AT/deg, Rmi/cm, Rma/cm, RM/cm,'
     >//' NR, dR/cm, NX, dX/cm, dA/rd : '
      write(2,fmt='(a,1p,5(e16.8,1x),2(i3,1x,e16.8,1x),e16.8)')
     >'# ',AT, AT/pi*180.d0,Rmi, Rma, RM, NR, dR, NX, dX, dA
      write(2,*) '# For TOSCA:  315 121 1 22.1 1.  !IZ=1 -> 2D ; '
     >//'MOD=22 -> polar map ; .MOD2=.1 -> one map file'
      write(2,*) '# R*cosA (A:0->360), Z==0, R*sinA, BY, BZ, BX '
      write(2,*) '# cm                 cm    cm      kG  kG  kG '
      write(2,*) '# '

      do jr = 1, NR
        R = Rmi + dble(jr-1)*dR
        do ix = 1, NX
          A = A1 + dble(ix-1)*dA
```

```
C         write(2,fmt='(1p,6(e16.8),a)')  R, Z, A, BR, BZ, BA
          X = R * sin(A)
          Y = R * cos(A)
          write(2,fmt='(1p,6(e16.8),a)')  Y, Z, X, BY, BZ, BX
        enddo
      enddo

      stop ' Job complete ! Field map stored in geneSectorMap.out.'
      end
```

Zgoubi input data file

```
A uniform field 180 degree sector dipole field map in cylindrical coordinates,
! used twice so to simulate a 360 degree cyclotron dipole.
! A 200 keV proton is tracked through. Its step-by-step coordinates are logged to zgoubi.plt.
 'OBJET'
64.62444403717985                                        ! Rigidity (kG.cm), 200keV proton.
2
1 1
12.9248888074 0. 0. 0. 0. 1. 'm'            ! Injection radius (all other coordinates zero).
1

 'PARTICUL'              ! This is required only because we want to get the time-of-flight,
938.27208 1.602176487D-19 1.79284735 0. 0.    ! raytracing otherwise just requires rigidity.
! PROTON                                                ! An alternate way to define a proton.

 'FAISTORE'
zgoubi.fai   #End       ! #End tells where (at which subsequent labeled keyword), particle
1                       ! data are to be logged to zgoubi.fai.
 'TOSCA'                ! First 180 degree field map
0  2                    ! IL=2 here logs the step-by-step proton coordinates to zgoubi.plt.
1.  1. 1. 1.
HEADER_8
315 121 1 22.1 1.       ! IZ=1 -> 2D ; MOD=22 -> polar map ; .MOD2=.1 -> single map.
geneSectorMap.out
0 0 0
2                       ! 9*9 node grid for second order fiel interpolation.
1.                      ! 1 cm step size.
2
0. 0. 0. 0.
 'TOSCA'                ! Second 180 degree field map
0  2                    ! IL=2 here logs the step-by-step proton coordinates to zgoubi.plt.
1.  1. 1. 1.
HEADER_8
315 121 1 22.1 1.       ! IZ=1 -> 2D ; MOD=22 -> polar map ; .MOD2=.1 -> single map
geneSectorMap.out
0 0 0 0
2                       ! 9*9 node grid for second order fiel interpolation
1.                      ! 1 cm step size
2
0. 0. 0. 0.

 'FAISCEAU'  #End       ! Label '#End' tells 'FAISTORE' to log particle data here!
 'END'
```

1.5.2 *Optical sequence for Exercise 1.2.1-1.c*

The cyclotron is defined using a mathematical model for the dipole field, a 60 degree sector, here. This optical sequence can be copy-pasted to a Zgoubi input data file and run as it is.

```
Cyclotron, classical.
 'OBJET'
64.62444403717985                               ! 200keV
2
4 1
12.9248888074 0.  0.   0.   0.  1. 'm'          ! 200keV. R=Brho/B=*/.5
28.9070891209 0.  0.   0.   0.  2.23654451125 'm'   ! 1 MeV. R=Brho/B=*/.5
50.           0.  0.   0.   0.  3.86850523397 'o'   ! at RM  (B*rho=0.5*0.5=0.25T.m, 2.9885 MeV)
64.7070336799 0.  0.   0.   0.  5.0063899693  'M'   ! 5 MeV. R=Brho/B=*/.5
1 1 1 1

 'DIPOLE'
0
60. 50.
30.  5. 0. 0. 0.
```

```
0.  0.                                          ! EFB 1  hard-edge
4  .1455   2.2670  -.6395  1.1558  0. 0.  0.
30. 0.  1.E6  -1.E6  1.E6  1.E6
0.   0.                                         ! EFB 2
4  .1455   2.2670  -.6395  1.1558  0. 0.  0.
-30. 0.  1.E6  -1.E6  1.E6  1.E6
0. 0.                                           ! EFB 3
0  0.      0.      0.      0.      0. 0.  0.
0. 0.  1.E6  -1.E6  1.E6  1.E6 0.
4   10.
1.                ! The smaller, the better the orbits close.
2  0. 0. 0. 0.    ! Could also be, e.g., 2 50. 0. 50. 0. with Y0 amended accordingly in OBJET
 'FAISCEAU'
 'FAISTORE'
 zgoubi.fai
 1
 'END'
```

Bibliography

[1] E.O.Lawrence and N.E.Edlefsen, Science 72, 376 (1930);
E.O.Lawrence and M.S. Livingston, Phys. Rev. 37 (1931), 1707; 38, 136, (1931); 40, 19 (1932)
[2] T. Kawaguchi et al., Design of the sector magnets for the RIKEN superconducting ring cyclotron, Proceedings of the 15th International Conference on Cyclotrons and their Applications, Caen, France.
http://www.nishina.riken.jp/facility/SRC_e.html
[3] H.A.Bethe and M.E.Rose, Phys. Rev. 54, 588 (1938)
[4] L.H.Thomas, *The Paths of Ions in the Cyclotron*, Phys. Rev. 54, 580, (1938)
[5] F. Chautard, *Beam Dynamics For Cyclotrons*, in *CERN Accelerator School*, Zeegse, The Netherlands, 24 May-2 June 2005.
[6] J. Le Duff, *Longitudinal beam dynamics in circular accelerators*, in *CERN Accelerator School*, Jyvaskyla, Finland, 7-18 September 1992.
[7] T. Stammbach, *Introduction to Cyclotrons*, in *CERN accelerator school, cyclotrons, linacs and their applications*, IBM International Education Centre, La Hulpe, Belgium, 28 April-5 May 1994.
[8] H. A. Enge, Deflecting magnets, in Focusing of Charged Particles, Vol. 1, A. Septier Ed., Academic Press (1967).
[9] G. Leleux, Circular accelerators, INSTN lectures, SATURNE Laboratory, CEA Saclay (Juin 1978). Some passages of the present document are inspired from these lectures.